Macromolecules

Article

Cite This: Macromolecules 2018, 51, 4370−4380

Effect of the Ratio l_K/p on Glassy-Polymeric Shear Deformation Mechanisms

Hong T. Nguyen and Robert S. Hoy*

Department of Physics, University of South Florida, Tampa, Florida 33620, United States

ABSTRACT: Using molecular dynamics simulations, we study how chain stiffness affects how glassy polymers deform under applied shear. Loosely entangled systems composed of flexible chains exhibit strong shear banding and subsequent strain softening whereas tightly entangled systems composed of semiflexible chains exhibit neither of these. For all systems, inflection points in stress−strain curves correspond to the onset of chain scission, but nonlinear strain hardening continues up to much larger strains. Tightly entangled systems build up considerable elastic energy before fracturing via chain scission. This causes their plastic flow to be far more heterogeneous, and they ultimately fail along significantly sharper fracture planes than their loosely entangled counterparts, which fail via chain pullout. We quantify these differences using modern plasticity metrics and relate them to chain-stiffness-dependent differences in segmental packing efficiency and interchain interpenetration. It appears that the additional stress transmission mechanisms provided by the greater covalent bond tensions present in tightly entangled systems act to delocalize strain and promote more homogeneous deformation than is found in loosely entangled systems, but only until chain scission begins.

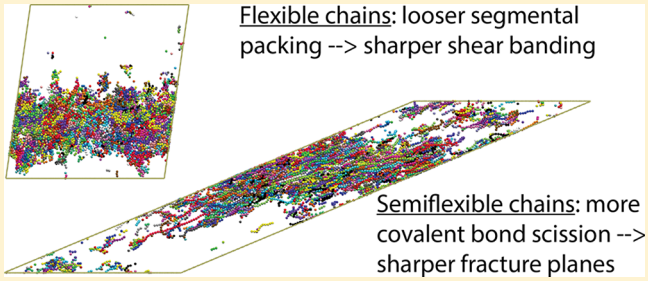

1. INTRODUCTION

Experimental studies comparing the drastically different mechanical responses of chemically different polymer glasses have a long history.[1−5] Many of the most basic features, such as tighter entanglement promoting ductility while greater aging promotes brittleness, are reasonably well understood. Far less well understood, however, is how these trends relate back to systems' molecular architecture and microscopic interactions as well as how they relate to differences in the character of systems' deformation micromechanisms.

One obstacle to obtaining better understanding of these issues is that although polymeric systems' entanglement density ρ_e, melt plateau modulus G_N^0, and glassy strain hardening modulus G_R all scale as $(l_K/p)^3$, where l_K and p are respectively their Kuhn and packing lengths,[6−11] and it is well-known that higher entanglement density stabilizes systems against strain localization and brittle failure,[12−14] it is difficult to relate these trends directly to chain stiffness because variable chain *thickness* (i.e., the presence of bulky side chains in some polymers but not others) obscures the relationship between chain stiffness and ρ_e.[15−18] Thus, although increasing chain stiffness usually increases both ρ_e and toughness,[4,5,16] counterexamples exist; e.g., polystyrene is less entangled and more brittle than polycarbonate even though polystrene is the stiffer polymer.

Another source of difficulty is that traditional theoretical approaches[1,13,19,20] treat systems as spatially homogeneous, ignoring the structural heterogeneity that has since been shown to be a key feature controlling the mechanical response of both nonpolymeric[21,22] and polymeric glasses.[23−25] Thus predicting even basic material properties such as whether a given system will be brittle or ductile remains a focus of intense current research interest,[25−27] and theoretical design of materials with optimized mechanical response—in particular, materials which preferentially fail via homogeneous shear—remains a largely unrealized goal.[11,28]

Recent years have seen a profusion of simulation studies of the micromechanisms of glassy plasticity. Multiple metrics characterizing the spatiotemporal structure of plastic events have been developed and successfully related (at a predictive level) to systems' microstructure.[21,22,29−34] However, while it has long been known that polymer glasses' plastic-deformation micromechanisms depend in detail on their microstructure (both intrachain and interchain[1,3]), application of these modern plasticity metrics to improving our understanding of their nonlinear shear response has only just begun.[35]

In this paper, using molecular dynamics simulations of a standard coarse-grained bead−spring polymer model,[36] we study how the shear response of model polymer glasses depends on chain stiffness for *fixed* chain thickness. By varying l_K/p with all other system properties held fixed—an operation which is very difficult to achieve in experiments—we isolate the role played by this critical parameter. Our results accord with established views of how chain stiffness influences shear deformation by controlling both segment-scale packing efficiency and the tightness of the entanglement mesh,[8,12,13] but go significantly beyond previous work by clarifying how

Received: March 27, 2018
Revised: May 9, 2018
Published: June 1, 2018

DOI: 10.1021/acs.macromol.8b00651
Macromolecules 2018, 51, 4370−4380

these relate to systems' heterogeneous microstructure and heterogeneous microscale plastic deformation.

2. MODEL AND METHODS

We employ the widely used Kremer–Grest bead–spring model,[36] which has been shown to capture many features of glassy-polymeric mechanical response.[25,37] Systems are composed of $N_{ch} = 500$ linear chains of $N = 600$ monomers. Periodic boundary conditions are applied along all three directions of (initially) cubic simulation cells. All monomers have mass m and interact via the truncated and shifted Lennard-Jones potential

$$U_{LJ}(r) = 4\epsilon\left[\left(\frac{a}{r}\right)^{12} - \left(\frac{a}{r}\right)^{6} - \left(\frac{a}{r_c}\right)^{12} + \left(\frac{a}{r_c}\right)^{6}\right] \quad (1)$$

where ϵ is the intermonomer binding energy, a is monomer diameter, and $r_c = 2^{7/6}a$ is the cutoff radius. The Lennard-Jones time unit is $\tau = \sqrt{ma^2/\epsilon}$, and the MD time step employed is $\delta t = \tau/200$. All molecular dynamics simulations are performed using LAMMPS.[38]

Simulations are conducted in three stages: (i) melt equilibration at $T > T_g$; (ii) slow cooling to $T = 0$; (iii) applied shear deformation at $T = 0$. In stage (i), covalent bonds connecting consecutive monomers along chain backbones are modeled using the FENE potential $U_{FENE}(r) = -(kR_0^2/2)\ln[1 - (r/R_0)^2]$, with the standard[36] parameters $k = 30\epsilon/a^2$ and $R_0 = 1.5a$. Systems are thoroughly equilibrated[39] at constant (zero) pressure at $T = T_g + 0.1\epsilon/k_B$, with pressure controlled using a Nosé–Hoover barostat. Note that the lower-than-usual equilibration temperature employed here is chosen because doing so is necessary to properly equilibrate the large-scale chain structure (and the entanglement length N_e) for semiflexible chains.[40,43] Values of T_g for all systems are given in Table 1.

In stage (ii), the covalent bond potential is switched to a quartic form suitable for studies of fracture:

$$U_{qu}(r) = U_0 + k_q(r - R_b)^3(r - R_b - B_2) \quad (2)$$

Bonds break when their length exceeds $R_b = 1.3a$. Following ref 45, B_2 is selected by matching $U_{qu}(r)$ to the first zero and the minimum of U_{FENE}, which sets $B_2 = -0.4668a$. Motivated by experimental data and previous bead–spring studies of glassy-polymeric fracture,[37,41] the ratio of the forces at which covalent and van der Waals bonds break is set to 100 by setting $k_q = 9640\epsilon/a^4$. In order to minimize the effect of slow dynamics near the glass transition on the low-T mechanical properties that are our primary interest, all systems are cooled from $T = T_g + 0.1\epsilon/k_B$ to $T = T_g - 0.1\epsilon/k_B$ at a very slow rate ($|\dot{T}| = 10^{-6}/\tau$) before continuing cooling to $T = 0$ at $|\dot{T}| = 10^{-5}/\tau$. This protocol produces fairly well-aged[46] glasses that can exhibit significant strain softening[47,48] and hence should readily shear band if the constituent chains' intrinsic properties (i.e., their microscopic interactions) support this.

In stage (iii), systems are sheared in the yz-plane at a constant engineering strain rate $\dot{\gamma} = 2.5 \times 10^{-4}/\tau$. This rate is low enough to be in the quasistatic regime[49] where stresses vary logarithmically with $\dot{\gamma}$; lower strain rates do not qualitatively change the results presented below. To mimic experiments, the stress along the x-direction (σ_{xx}) is maintained at zero thoughout the deformation runs. This protocol allows volume changes during deformation, which is critical since dilatation has long been known to be critical in controlling shear banding in amorphous materials.[50] All systems are strained up to and slightly beyond the fracture strain γ_{frac} (the strain at which the shear stress σ_{yz} is maximized).

In all stages, angular interactions between three consecutive beads along chain backbones are modeled using the standard potential[39]

$$U_b(\theta) = k_{bend}(1 - \cos(\theta)) \quad (3)$$

where θ_i is the angle between consecutive bond vectors $\vec{b}_i$ and $\vec{b}_{i+1}$; here $\vec{b}_i = \vec{r}_{i+1} - \vec{r}_i$ and $\vec{r}_i$ is the position of bead i. Note that θ is zero and U_b is minimized for straight trimers. We consider three chain stiffnesses ranging from flexible ($k_{bend} = 0$) to fairly stiff ($k_{bend} = 4\epsilon$). Most previous studies have focused on $k_{bend} \leq 2\epsilon$.[25,37,42,51] Our $k_{bend} = 4\epsilon$ chains are well into the semiflexible regime where l_K is comparable to the tube diameter d_T, producing entanglement that is qualitatively different from that found in flexible chains.[52]

The chain stiffnesses considered here are too low to produce long-range nematic order. However, short-range nematic order can also strongly affect mechanical properties. We characterize such short-range order via the methods employed in ref 53. The order parameter S is given by

$$S = \left\langle \sqrt{\frac{3}{2}\mathrm{Tr}(\bar{q}\cdot\bar{q})} \right\rangle \quad \text{where } q_{\alpha\beta} = \left\langle \hat{b}_\alpha\hat{b}_\beta - \frac{1}{3}\delta_{\alpha\beta} \right\rangle \quad (4)$$

Here Tr is the trace operator, the $\langle ... \rangle$ denote averaging over all cubic subcells of side length $\sim 3a$ and averaging of all normalized bond vectors $\hat{b} = \vec{b}/|\vec{b}|$ in each such subcell, and $\hat{b}_\alpha$ and $\hat{b}_\beta$ are Cartesian components of $\hat{b}$. In eq 4, $S = 0$ ($S = 1$) correspond to covalent bonds being perfectly unaligned (perfectly aligned) within each subcell. We find that in the glassy state S ranges from $\simeq 0.3$ for flexible chains to $\simeq 0.45$ for $k_{bend} = 4\epsilon$ chains, with only a very weak T-dependence. This indicates that—as expected—neighboring covalent backbones are more aligned for stiffer chains. However, the magnitude of this effect is small. It only becomes large when midrange nematic order (order over distances $\gtrsim 2a$) develops, i.e., for $k_{bend} \gtrsim 5\epsilon$.[53] Thus, we claim that the differences in systems' mechanical response reported below have little to do with differences in their nematic order. We have also verified that all systems remain amorphous; i.e., increasing k_{bend} does not produce any long-range positional order.

We quantitatively characterize plastic deformation during stage (iii) using Falk and Langer's nonaffinity measure D^2_{min}.[29] For each monomer i, D^2_{min} is defined as the local deviation from

Table 1. Glass Transition Temperatures and Statistical Properties of Chains at $T = 0$[a]

k_{bend}/ϵ	$k_B T_g/\epsilon$	C_∞	N_e
0	0.37	1.74	70
2	0.47	5.31	15
4	0.60	6.89	14

[a]The entanglement length N_e is obtained by primitive path analysis (PPA).[10] These values of N_e are slightly smaller than those reported in the literature for $k_BT = \epsilon$,[10,44] but are consistent with the idea that entanglements in the glassy state are inherited from the $T \simeq T_g$ supercooled melt[1] and reflect the fact that for our chosen $U_b(\theta)$ chains straighten with decreasing T (which in turn decreases N_e[43]).

DOI: 10.1021/acs.macromol.8b00651
Macromolecules 2018, 51, 4370–4380

affine deformation of the monomer's "neighborhood" (the set of all n_i monomers j such that $|\vec{r}_j - \vec{r}_i| < r_c$) over the strain interval $[\overline{\gamma} - \Delta\overline{\gamma}, \overline{\gamma}]$, i.e., over the tensorial strain increment $\Delta\overline{\gamma}$:

$$D^2_{\min,i} = \min[(n_i^{-1}\sum_{j=1}^{n_i}\sum_{\alpha}[\vec{r}_{ji}(\overline{\gamma})\cdot\hat{u}_\alpha - \sum_{\beta}(\delta_{\alpha\beta} + \Delta\epsilon_{\alpha\beta})(\vec{r}_{ji}(\overline{\gamma} - \Delta\overline{\gamma})\cdot\hat{u}_\beta)])2]_{\Delta\overline{\epsilon}} \quad (5)$$

Here α and β denote the Cartesian directions x, y, z, $\hat{u}_\alpha$ is the unit vector along direction α, and $\vec{r}_{ji} = \vec{r}_j - \vec{r}_i$. $\Delta\overline{\gamma}$ is the strain occurring over the applied shear strain increment $\Delta\gamma = 5 \times 10^{-3}$; this increment is small enough that multiple plastic rearrangements of a single region rarely occur. As in ref 29, plastic deformation is quantified by finding the tensorial strain increment $\Delta\overline{\epsilon}$ that minimizes $D^2_{\min,i}$. In general, $\Delta\overline{\epsilon} \neq \Delta\overline{\gamma}$, and the degree of nonaffinity has been shown in many studies (e.g., refs 22, 29, 32, and 35) to correlate well with the degree of plastic activity.

3. RESULTS

Figure 1a shows the stress−strain curves $\sigma_{yz}(\gamma)$ for all systems. Results at small strains are consistent with many previous studies; an elastic response at small strains is followed by yielding, plastic flow, and strain hardening that becomes more dramatic (nonlinear) as γ increases.[40] This degree of nonlinearity is far greater for the more tightly entangled semiflexible-chain systems due to the same factors discussed elsewhere (e.g., in refs 54−56); stretching of chains between entanglements both stores energy and increases plastic activity. The $\sigma_{yz}(\gamma)$ curves have inflection points (switch from concave-up to concave-down) at characteristic strains $\gamma_{\text{infl}}(k_{\text{bend}})$ (Table 2) that decrease strongly with increasing chain stiffness.[42] At larger strains, stress continues to increase—albeit with negative $d^2\sigma_{yz}/d\gamma^2$—until systems fracture at $\gamma \simeq \gamma_{\text{frac}}$. As expected, values of γ_{frac} also decrease strongly with increasing chain stiffness. Note that the slow stress decrease shown for $\gamma > \gamma_{\text{frac}}$ is an artifact of the periodic boundary conditions (PBCs) employed here. PBCs are well-known to artificially suppress catastrophic failure, but eliminating this effect by making systems nonperiodic along one or more directions produces spuriously large surface effects for all currently computationally feasible system sizes. Thus, we focus on $\gamma \lesssim \gamma_{\text{frac}}$ for the remainder of this paper.

As expected,[42,51] the inflection points in $\sigma_{yz}(\gamma)$ correspond closely to the onset of bond scission. Figure 1b shows the fraction of broken covalent bonds $f_{\text{brok}}(\gamma)$ for the same systems. $f_{\text{brok}}(\gamma)$ is small for $\gamma < \gamma_{\text{infl}}$ and then rises sharply until systems fracture. Figure 1b also shows that the ultimate fraction of broken bonds grows sharply as chain stiffness increases and that the qualitative behavior of $f_{\text{brok}}(\gamma)$ in $k_{\text{bend}} \geq 2\epsilon$ systems is different from its behavior in flexible-chain systems. For $k_{\text{bend}} \geq 2\epsilon$, the bond scission rate $df_{\text{brok}}/d\gamma$ peaks at $\gamma \simeq \gamma_{\text{frac}}$, indicating that chain scission is the primary failure mode in these systems. In flexible-chain systems, no such peak in $df_{\text{brok}}/d\gamma$ is present. Instead, $df_{\text{brok}}/d\gamma$ increases at $\gamma \simeq \gamma_{\text{frac}}$. We will show below that this occurs because these systems are failing via chain *pullout*.

Figure 1c shows systems' fractional volume change $V(\gamma)/V_0 - 1$ during the deformation. All systems increase their volume during deformation by expanding along the transverse (x) direction. However, these increases differ strongly in both kind and degree. Dilatation has long been associated with shear banding.[13,50] Here, flexible-chain systems dilate relatively rapidly at low strains. This stronger dilatation leads to the more dramatic yielding at $\gamma = \gamma_{\text{yield}}$ shown in the inset of panel

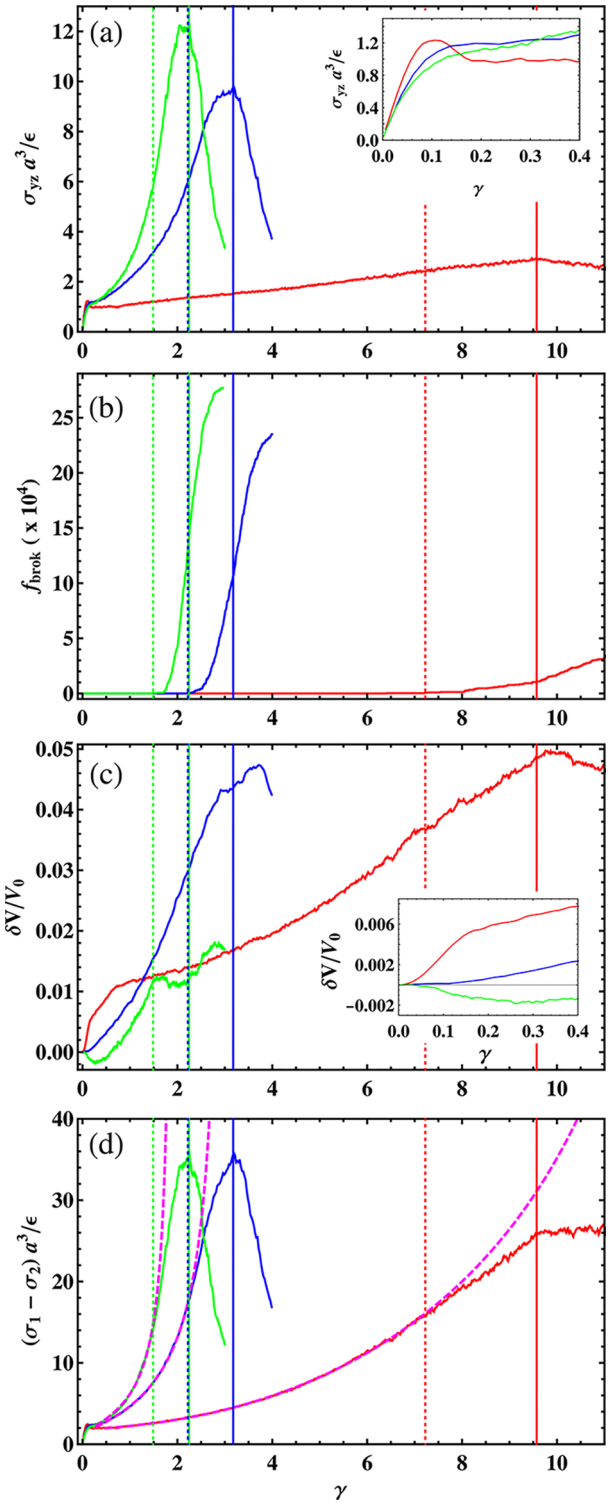

Figure 1. Basic features of mechanical response: (a) shear stress σ_{yz}, (b) fraction of broken bonds, (c) fractional volume change, and (d) principal stress difference $[\sigma_1 - \sigma_2]$ as a function of nominal shear strain γ for three different chain stiffnesses. Red, blue, and green respectively indicate data for systems with k_{bend}/ϵ = 0, 2, and 4. Vertical dotted lines indicate the onset of bond scission at $\gamma = \gamma_{\text{infl}}$ for each k_{bend}, while vertical solid lines indicate the fracture strains γ_{frac}.[40] The insets to panels a and c highlight the response in the small-strain regime, and the dashed magenta curves in panel d show fits to the eight-chain model (eq 6).

DOI: 10.1021/acs.macromol.8b00651
Macromolecules 2018, 51, 4370−4380

Table 2. Characteristic Strains γ_{yield}, γ_{infl}, γ_{frac}, and γ_{crit} for Simple Shear Deformation at $\dot{\gamma} = 2.5 \times 10^{-4}/\tau$[40]

k_{bend}/ϵ	γ_{yield} [a]	γ_{infl}	γ_{frac}	γ_{crit} (eq 8)
0	0.104	7.22	9.57	10.85
2	0.154	2.22	3.18	2.34
4	0.154	1.49	2.24	1.76

[a]Values of γ_{yield} are identified by finding the strains at which $d\sigma_{yz}/d\gamma$ is zero (for flexible chains) or locally minimal (for semiflexible chains).

Table 3. Fit Parameters to the Eight-Chain Model (Eq 6) Obtained from the Stress−Strain Curves Shown in Figure 1d

k_{bend}/ϵ	τ_{12}^{flow} (ϵ/a^3)	G_R (ϵ/a^3)	N_e
0	1.745	0.223	136
2	1.274	1.197	22
4	1.261	1.176	16

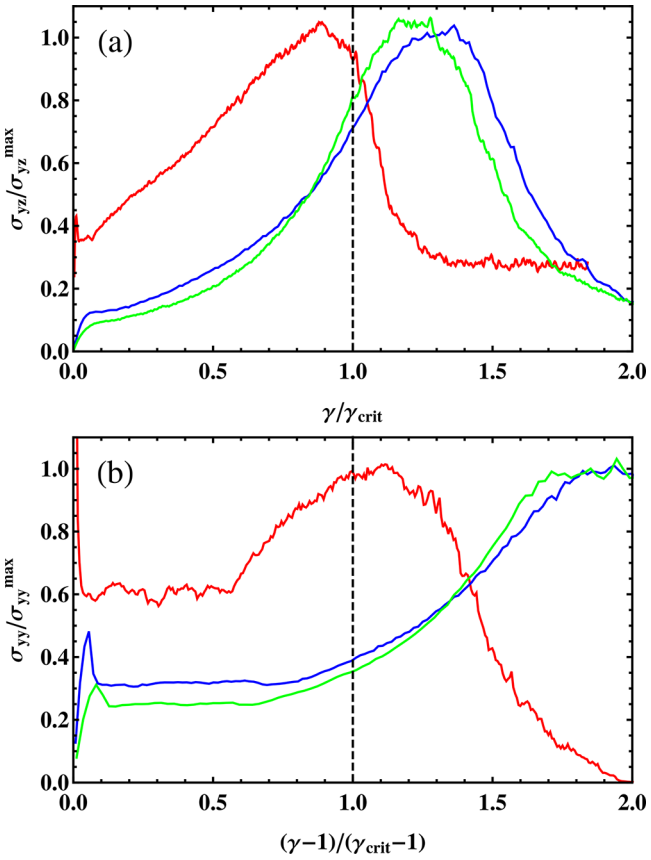

Figure 2. Scaled stress−strain curves. Red, blue, and green respectively indicate data for systems with k_{bend}/ϵ = 0, 2, and 4. (a) The same results as in Figure 1a, but with strains scaled by $\gamma_{crit}(k_{bend})$ (eq 8; Table 2) and stresses scaled by the maximal values $\sigma_{yz}^{max} = \sigma_{yz}(\gamma_{frac})$. (b) The corresponding results for crazed systems where crazing is induced by uniaxial-strain extension. For this protocol, γ is uniaxial *stretch*, and γ_{crit} = 10.9, 2.5, and 2.0 for k_{bend} = 0, 2ϵ, and 4ϵ.

a; we will show below that these trends are associated with formation of a "sharp" shear band. In contrast, intermediate-flexibility (k_{bend} = 2ϵ) systems deform at nearly constant volume prior to yielding, but dilate more strongly in the strain-hardening regime, while stiffer (k_{bend} = 4ϵ) chains exhibit much weaker dilatation. These differences are consistent with the lack of clear yielding and strain softening in these systems and suggest that their deformation is more homogeneous (at least for $\gamma \lesssim \gamma_{yield}$). Below we will relate these differences to differences in systems' strain localization and fracture micromechanisms in much more detail.

The eight-chain model of Arruda and Boyce[57] has long been used to model glassy-polymeric deformation because it is mathematically simple yet can accurately capture stress−strain relations (including the nonlinear-hardening regime) for a wide variety of deformation modes.[57,58] It predicts the stress difference between the principal stress components σ_i and σ_j to be

$$\sigma_i - \sigma_j = \tau_{ij}^{flow} + G_R \frac{\mathcal{L}^{-1}(h)}{3h}(\lambda_i^2 - \lambda_j^2) \quad (6)$$

where τ_{ij}^{flow} is a plastic flow term, G_R is the strain hardening modulus, λ_i and λ_j are the principal stretches along directions i and j, $h = \lambda_{chain}/(N_e/C_\infty)^{1/2}$ where $\lambda_{chain} = [(\lambda_1^2 + \lambda_2^2 + \lambda_3^2)/3]^{1/2}$ describes the increase in chains' mean end−end distance $\langle R_{ee}^2\rangle^{1/2}$ during deformation, and $\mathcal{L}^{-1}$ is the inverse Langevin function.[57] Neglecting the small volume changes shown in panel c, the principal stretches are $\lambda_1 = (\sqrt{\gamma^2+4} + \gamma)/2$, $\lambda_2 = (\sqrt{\gamma^2+4} - \gamma)/2$, and $\lambda_3 = 1$. Stress is purely tensile along the λ_1-axis and purely compressive along the λ_2-axis; see Figure 3a for a schematic diagram of how these relate to our simulation geometry. In our simple shear deformation protocol, the stress tensor $\bar{\sigma}$ has only four nonvanishing components: σ_{yy}, σ_{zz}, and $\sigma_{yz} \equiv \sigma_{zy}$. The two principal stresses (i.e., the stresses along the above-mentioned principal stretch directions 1, 2) are given by

$$\sigma_{1,2} = (\sigma_{yy} + \sigma_{zz})/2 \pm \sqrt{(\sigma_{yy} - \sigma_{zz})^2/4 + \sigma_{yz}^2} \quad (7)$$

Figure 1d shows the stress differences $[\sigma_1 - \sigma_2](\gamma)$ together with fits to the eight-chain model for all systems. The fit parameters τ_{12}^{flow}, G_R, and N_e are given in Table 3. As in previous studies,[9,11,55] the fit values of N_e are in general inconsistent with those obtained from rheological measurements and topological analyses. Nevertheless, if the fits are restricted to the strain range $\gamma_{yield} < \gamma \leq \gamma_{infl}$, eq 6 quite accurately captures the shape of the stress−strain curves. The dashed magenta curves in Figure 1d are fit over this range but are extended to larger γ in the plot to illustrate how the breakdown of the eight-chain model nicely coincides with the onset of bond scission. Since the character of the stresses in the different systems considered here become quite different for $\gamma \gg \gamma_{yield}$—for example, the stresses associated with bond tension grow large in tightly entangled semiflexible-chain systems but not in loosely entangled flexible-chain systems[56]—the success of the eight-chain model[57,58] in capturing the shapes of stress−strain curves over such a wide range of γ is rather remarkable.

The three systems considered here fracture at very different stress and strain levels. One way of comparing them on a more equal footing is to plot their mechanical response in appropriately scaled fashion. Figure 2a shows the shear stresses σ_{yz} scaled by their maximum values $\sigma_{max} = \sigma_{yz}(\gamma_{frac})$ and plotted against the scaled shear strain γ/γ_{crit}. Here γ_{crit} is the strain at which initially Gaussian chains of characteristic ratio C_∞ and entanglement length N_e (with uniformly spaced entanglements and no chain slippage during deformation) pull taut. Its value for each system is given by the solution to the equation

$$\lambda_1^2(\gamma_{crit}) + \lambda_2^2(\gamma_{crit}) + \lambda_3^2(\gamma_{crit}) = 3N_e/C_\infty \quad (8)$$

DOI: 10.1021/acs.macromol.8b00651
Macromolecules 2018, 51, 4370−4380

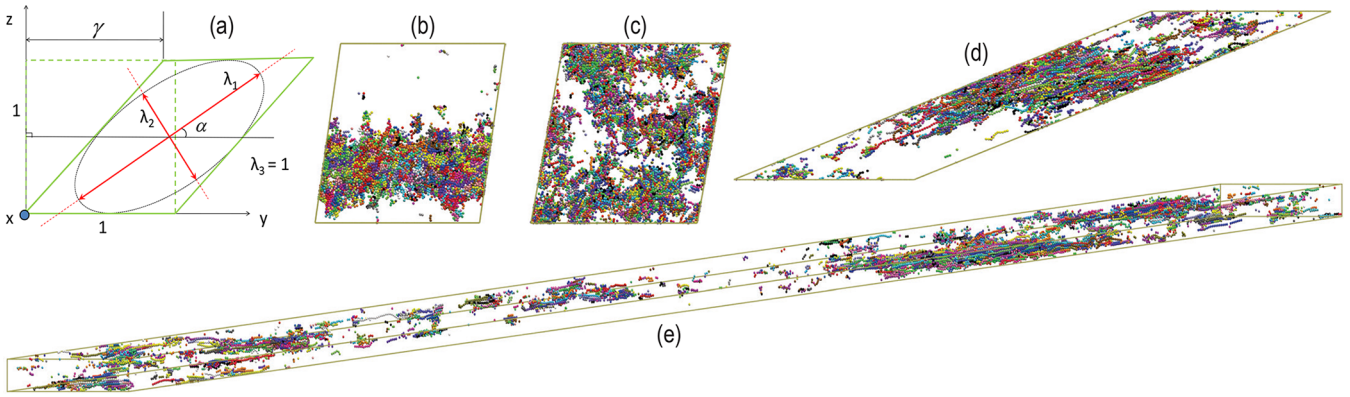

Figure 3. Spatial structure of plastic activity: (a) The shear geometry and principal strain directions. Note that the angle between the direction $(\hat{\lambda}_1)$ and the shear (xy) plane is $\alpha = \tan^{-1}(2/\gamma)$, while $\hat{\lambda}_1$ and $\hat{\lambda}_2$ remain perpendicular for all γ.[5] (b–e) The 5% most damaged (highest D^2_{min}) monomers for (b) $k_{bend} = 0$, $\gamma = \gamma_{yield}$; (c) $k_{bend} = 4\epsilon$, $\gamma = \gamma_{yield}$; (d) $k_{bend} = 4\epsilon$, $\gamma = \gamma_{frac}$; (e) $k_{bend} = 0$, $\gamma = \gamma_{frac}$. Panel e is rotated to illustrate the fact that in there is no "fracture plane" of highly damaged atoms spanning the system. In panels b–e, monomers belonging to different chains are assigned different colors. Images were created using VMD.[61]

for the above-mentioned principal stretches $(\lambda_1, \lambda_2, \lambda_3)$.

The scaled stresses for tightly entangled, semiflexible-chain systems evolve similarly with increasing scaled strain; both systems fracture at $\gamma \simeq 1.1\gamma_{crit}$. A uniformly cross-linked network of Gaussian chains would fracture at $\gamma \simeq \gamma_{crit}$, shortly after chains pulled taut. Real networks can be deformed to slightly higher strains without fracturing because of strand dispersity,[59,60] and in uncrosslinked glasses, further deformation is allowed by chain slippage. Note that the γ_{crit} values predicted by eq 8 may underestimate the strain at which chain tension starts increasing ahead of fracture in $k_{bend} \geq 2\epsilon$ systems because the end–end vectors of successive entangled segments are finitely correlated in these tightly entangled systems, providing an additional stress-relief mechanism.[52,60] This is a subtle issue because eq 8's assumption that chains are Gaussian at chemical distances $n = N_e$ is only valid when $N_e \gg C_\infty$ (and as indicated in Table 1, this is not the case for our $k_{bend} \geq 2\epsilon$ systems). Nevertheless, it is clear that our $k_{bend} \geq 2\epsilon$ systems behave *roughly* like cross-linked networks; chains pull taut between entanglement points and then undergo scission. Flexible-chain systems, however, behave quite differently, fracturing at $\gamma \simeq 0.8\gamma_{crit}$. This is consistent with the argument given above—that flexible-chain systems fail via chain pullout rather than scission—and we will support it further below.

First, however, we will compare the results for shear shown in Figure 2a to their counterparts for crazing. The competition between crazing and shear is critical to understanding glassy-polymeric fracture and is closely associated with these systems brittle–ductile transition.[1,4,28,37] Figure 2b shows scaled stress–strain curves for crazing simulations wherein systems are extended uniaxially along the y direction at a rate $\dot{\gamma} = 2.5 \times 10^{-4}/\tau$ (where now $\gamma = L_y/L_y^0$ is the uniaxial stretch rather than the shear strain) with their transverse dimensions held constant.[41] The larger values of $\gamma_{frac}/\gamma_{crit}$ for crazing are consistent with experimental trends;[4] they arise from crazing's much more dilatative character, which allows for much greater chain slippage. More importantly in our present context, since the qualitative trends for craze failure are the same as they are for shear—less-entangled systems fail via chain pullout, at considerably lower values of γ/γ_{crit}—they should also remain the same under more general deformation protocols where crazing and shear can compete.[4,5,37]

The chain-stiffness-dependent differences discussed above can be elucidated by visualizing how deformation does (or does not) localize during shear. Figure 3 shows snapshots of the 5% most damaged (highest D^2_{min}) monomers for flexible and $k_{bend} = 4\epsilon$ systems at various strains. Panels b and c show results for $\gamma = \gamma_{yield}$. The flexible-chain system has a sharply defined shear band extending across the system, nearly parallel to the xy-plane. This shear band is clearly associated with the distinct yielding and strain softening shown in Figure 1a. In contrast, the tightly entangled $k_{bend} = 4\epsilon$ system shows no such shear banding. Instead, its plastic damage is diffuse and appears to be concentrated in the low-modulus, low-activation-energy "soft spots" discussed in many recent studies.[21,30,31,62–64]

Panels d and e show results for $\gamma = \gamma_{frac}$. The tightly entangled system fails at a sharply defined fracture plane. This highly damaged region possesses a much higher fraction of broken bonds than the surrounding, less damaged region. Excess bond scission in this region shortly prior to fracture causes more load to be borne by the remaining bonds, further increasing their scission rate and producing a local mechanical instability that leads to rapid catastrophic failure at the fracture plane. This picture is not novel—it is consistent with the standard view of chain-scission-dominated fracture[1]—but it provides a useful contrast to the very different behavior of loosely entangled systems. The much larger values of γ_{crit} in loosely entangled systems allow chains to become far more aligned prior to the onset of bond scission. Greater chain alignment is well known to reduce interchain friction in entangled polymer melts (see e.g. refs 65 and 66), and recent work has suggested that it also increases the effective tube diameter.[67] These factors in combination with these systems' greater dilatation (Figure 1c) strongly favor chain pullout over chain scission. As illustrated in panel e, failure of flexible-chain systems is not localized along a fracture plane but instead is rather homogeneous. This is consistent with the fact that chain pullout is a much less violent process because it occurs through breaking of van der Waals rather than covalent bonds. As such, chain pullout under applied shear deformation does not appear to induce the sort of sharp mechanical instability that favors strong strain localization.

A deeper understanding of such effects can be gained by examining how the statistical properties of plastic damage evolve during deformation (Figure 4). Panel a shows the mean

DOI: 10.1021/acs.macromol.8b00651
Macromolecules 2018, 51, 4370–4380

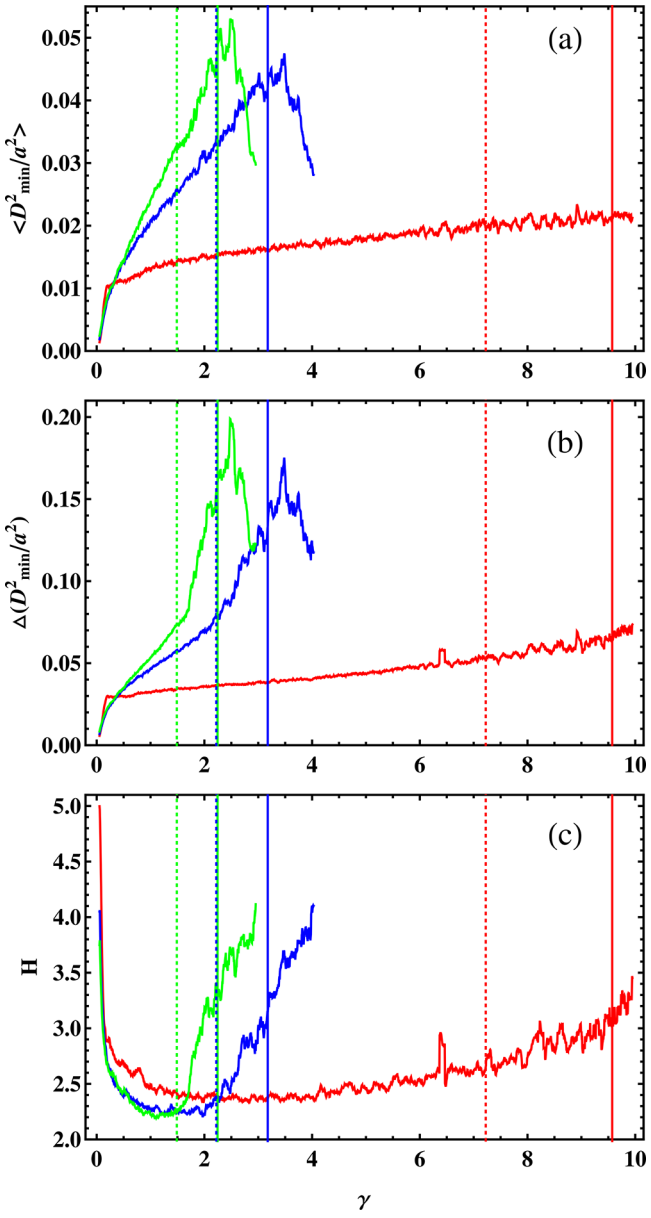

Figure 4. Statistical measures of plasticity. Red, blue, and green respectively indicate data for systems with k_{bend}/ϵ = 0, 2, and 4. (a) The mean nonaffinity $\langle D^2_{min}(\gamma)\rangle$ measured over strain intervals $\delta\gamma$ = 0.005. (b) The standard deviation $\Delta D^2_{min}(\gamma)$ of this measure. (c) The heterogeneity $H(\gamma) = \Delta D^2_{min}(\gamma)/\langle D^2_{min}(\gamma)\rangle$ of this measure. As in Figure 1, vertical dotted lines indicate $\gamma = \gamma_{infl}$ while vertical solid lines indicate $\gamma = \gamma_{frac}$. Note that the large "noise" in all panels is the result of the avalanche-like plasticity typical[22,34] of glasses deformed at low T.

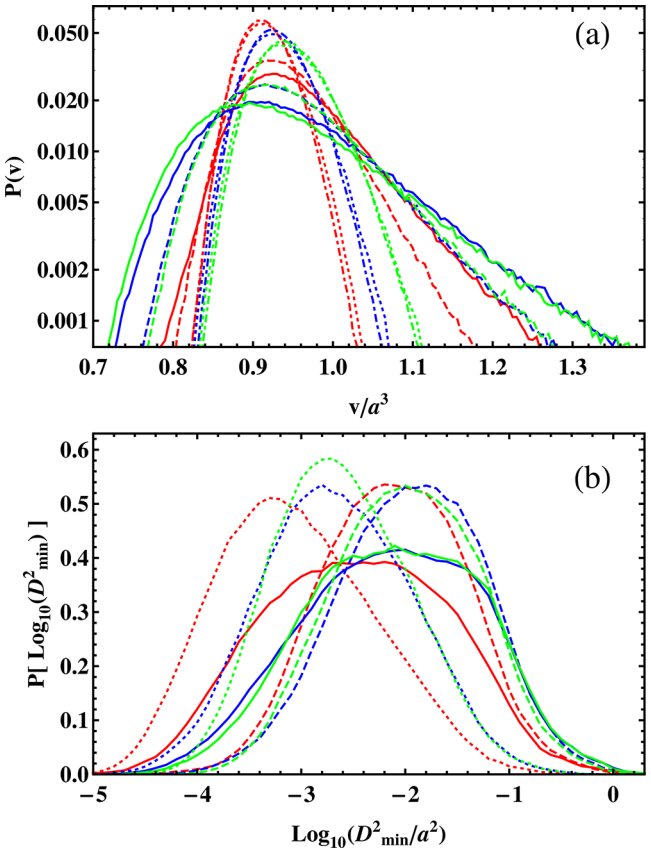

Figure 5. Connections between heterogeneous structure and heterogeneous plasticity. Red, blue, and green respectively indicate data for systems with k_{bend}/ϵ = 0, 2, and 4. (a) Voronoi volume distributions $P(v)$. (b) Nonaffinity distributions $P[\log(D^2_{min})]$. Both panels show results for $\gamma = \gamma_{yield}$ (dotted curves), $\gamma = \gamma_{infl}$ (dashed curves), and $\gamma = \gamma_{frac}$ (solid curves); panel a also shows results for undeformed systems (dash-dotted curves).

damage $\langle D^2_{min}(\gamma)\rangle$ for all systems. In all cases, $\langle D^2_{min}(\gamma)\rangle$ is roughly proportional to the macroscopic shear stress $\sigma_{yz}(\gamma)$ and more closely proportional to its dissipative component $\sigma^{diss}_{yz}(\gamma)$. The large fluctuations are present because the low-temperature limit we are considering here produces the avalanche-like plasticity common to all low-T glasses.[22,34] Similar trends have been observed for other deformation protocols such as uniaxial-stress and plane-strain compression.[55] Note that these fluctuations strengthen as strain rate decreases but are strongly suppressed as temperature increases.[68] It will be interesting in future work to see how such temperature- and rate-dependent effects couple to chain-stiffness effects—particularly since the strong strain-rate dependencies observed in experimental studies of shear fracture[28] imply that these couplings are strong.

Accounting for the fact that these systems' plastic deformation is *heterogeneous* provides additional insight. Panel b shows the standard deviation $\Delta D^2_{min}(\gamma) = [\langle (D^2_{min}(\gamma))^2\rangle - \langle D^2_{min}(\gamma)\rangle^2]^{1/2}$. At low strains, $\Delta D^2_{min}(\gamma)$ roughly tracks $\langle D^2_{min}(\gamma)\rangle$ and $\sigma^{diss}_{yz}(\gamma)$. At the onset of bond scission, however, $\Delta D^2_{min}(\gamma)$ begins increasing more sharply, indicating that plastic deformation is becoming more heterogeneous. This observation is strengthened by plotting the heterogeneity measure $H(\gamma) = \Delta D^2_{min}(\gamma)/\langle D^2_{min}(\gamma)\rangle$ (panel c). At low strains, $H(\gamma)$ is much greater in loosely entangled systems, consistent with the strong shear banding shown in Figure 3b. However, $H(\gamma)$ increases sharply upon the onset of chain scission at $\gamma = \gamma_{infl}$. Violent recoil from chain scission naturally leads to more-localized plastic damage and hence the higher $H(\gamma)$ for $\gamma > \gamma_{infl}$. This increase is far stronger for tightly entangled systems and continues through fracture. All trends are consistent with the more localized fracture observed in these systems (Figure 3d).

Next, in the spirit of many recent simulation studies of both nonpolymeric and polymeric glasses,[21,22,30−33,64] we attempt to relate the heterogeneity of these systems' plastic shear response to their structural heterogeneity. Since the long-standing assumption[50] that increasing local free volume eases shear deformation (and particularly shear banding) suggests that monomers with larger D^2_{min} should preferentially have higher

DOI: 10.1021/acs.macromol.8b00651
Macromolecules 2018, 51, 4370−4380

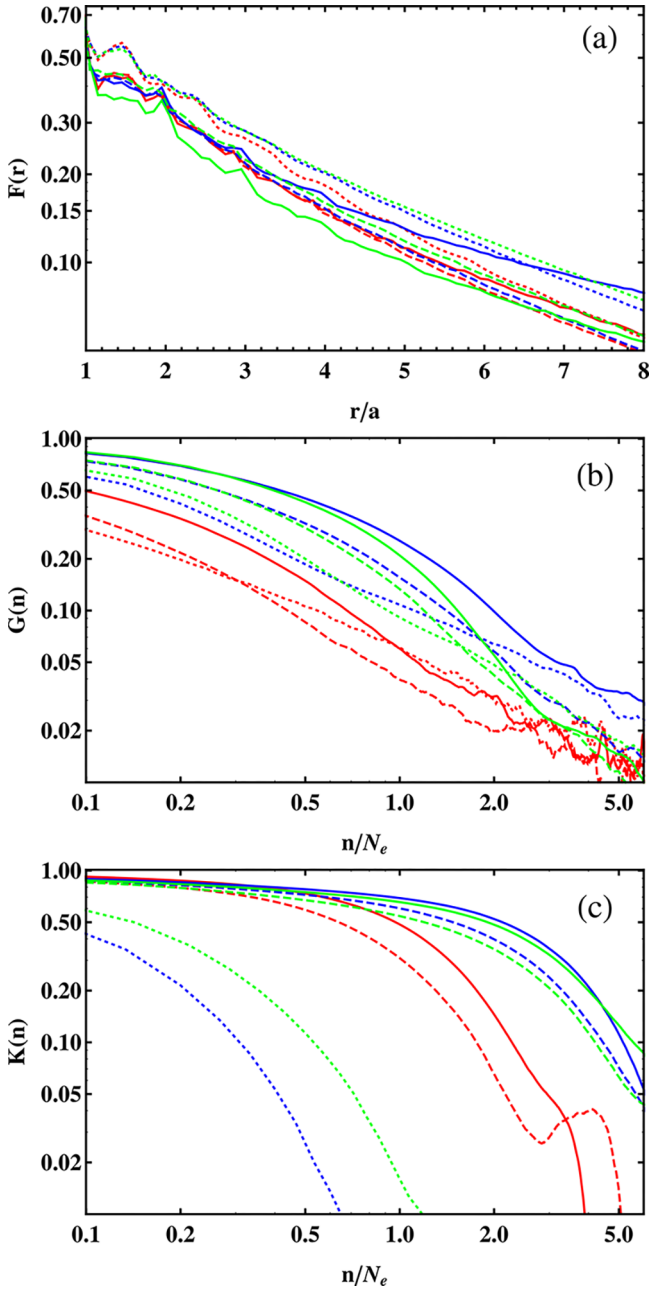

Figure 6. Additional measures of plasticity: Red, blue, and green respectively indicate data for systems with k_{bend}/ϵ = 0, 2, and 4. (a) Spatial correlations of D^2_{min} fluctuations ($F(r)$: eq 11). (b) Topological correlations of D^2_{min} fluctuations ($G(n)$: eq 12). (c) Topological correlations of covalent bond tension fluctuations ($K(n)$: eq 13). In all panels, dotted, dashed, and solid curves respectively show results for γ_{yield}, γ_{infl}, and γ_{frac}.

Voronoi volumes v before they rearrange, a particularly obvious spatially heterogeneous measure to examine is the Voronoi volume distribution.

Figure 5a shows the distributions of Voronoi volumes $P(v)$ in these systems. As is typical for glasses,[69] the distributions are roughly fit by

$$P(v) = A \exp\left(-\frac{(v - \langle v\rangle)^2}{2\sigma_v^2}\right) + f(v) \exp\left(-\frac{v}{v^*}\right) \quad (9)$$

where $f(v) \to 0$ for $v \ll \langle v\rangle$ and for $v \gg v^*$. The specific functional form of $f(v)$ is challenging to determine[69] but is not critical here. For $\gamma \lesssim \gamma_{yield}$, the distributions are close to Gaussian (small $f(v)$) and relatively narrow (small σ_v), albeit wider for semiflexible systems as expected from these systems' greater packing frustration.[70] At $\gamma \simeq \gamma_{yield}$, the distributions begin to broaden. In particular, the large-v contribution grows; $f(v)$ and v^* both increase. Surprisingly, the magnitudes of these increases for $\gamma \ll \gamma^{infl}$ are comparable for flexible-chain and semiflexible-chain systems even though the former shear-band while the latter do not. Once bond scission begins, however, the distributions broaden considerably more for semiflexible systems. Specifically, the low-v cutoff of $f(v)$ appears to soften, and v^* increases. This broadening reflects the violence of the bond scission process; postscission recoil naturally tends to create monomers with both low and high Voronoi volumes. Note that scission, in addition to being more prevalent in semiflexible systems (Figure 1b), is also more violent in these systems because of the greater strain energy released in individual scission events.

Figure 5b shows the distributions of D^2_{min} values at the characteristic strains γ_{yield}, γ_{infl}, and γ_{frac} (Table 2). These distributions have approximately log-normal form:

$$P(D^2_{min}) = \frac{\exp(-\Delta^2/2)/\sqrt{2\pi\Delta^2}}{\langle \log(D^2_{min})\rangle} \times \exp\left(-\frac{[\log(D^2_{min}) - \langle \log(D^2_{min})\rangle]^2}{2\Delta^2}\right) \quad (10)$$

Log-normal distributions often arise in amorphous plasticity, e.g., in the distributions of plastic-zone activation energies and plastic-event sizes.[34,71] They are very "fat-tailed" and indicate deformation physics dominated by rare, large, avalanche-like slip events.[34] In fits to the distributions plotted in panel b, $\Delta/\langle \log(D^2_{min})\rangle$ increases dramatically with γ as systems' plasticity becomes increasingly heterogeneous.

The natural question to ask, then, is whether the trends in $P(v)$ and $P(D^2_{min})$ with increasing shear strain are correlated and how any such correlations couple to other chain-stiffness effects. We calculated the Pearson's correlation coefficient $C(D^2_{min}, v) = \mathrm{cov}(D^2_{min}, v)/(\Delta D^2_{min}\, \Delta v)$, where $\mathrm{cov}(D^2_{min}, v)$ is the covariance of fluctuations of D^2_{min} and v while ΔD^2_{min} and Δv are their respective standard deviations, as a function of γ. $C(\gamma)$ increases with strain but remains small $[C(\gamma) \le 0.1]$ for all systems over the entire range $0 \le \gamma \le \gamma_{frac}$. Thus local plastic activity correlates only weakly with local free volume. While this lack of correlation accords with a previous study[64] that found cavitation under tensile deformation correlates only weakly with Voronoi volume, it seems inconsistent with traditional views[19,54] of the role free volume plays in the shear deformation of glassy polymers.

We also attempted to relate the differences in our systems' mechanical responses to differences in other metrics such as spatial correlations of D^2_{min}

$$F(r) = \frac{\langle D^2_{min}(\vec{r}_i) D^2_{min}(\vec{r}_i + \vec{r})\rangle - \langle D^2_{min}\rangle^2}{\langle (D^2_{min})^2\rangle - \langle D^2_{min}\rangle^2} \quad (11)$$

correlations of fluctuations in D^2_{min} along chain backbones

$$G(n) = \frac{\langle D^2_{min}(\vec{r}_i) D^2_{min}(\vec{r}_{i+n})\rangle - \langle D^2_{min}\rangle^2}{\langle (D^2_{min})^2\rangle - \langle D^2_{min}\rangle^2} \quad (12)$$

DOI: 10.1021/acs.macromol.8b00651
Macromolecules 2018, 51, 4370−4380

and correlations of covalent-bond-tension fluctuations along chain backbones

$$K(n) = \frac{\langle T(\vec{b}_i)T(\vec{b}_{i+n})\rangle - \langle T\rangle^2}{\langle T^2\rangle - \langle T\rangle^2} \quad (13)$$

(where $T = -\partial[U_{LJ}(r) + U_{qu}(r)]/\partial r$) that have proven useful in characterizing plastic deformation.[22,37,56] In eqs 11−13, n is the chemical distance and brackets indicate averaging over all monomers i.

Results are shown in Figure 6 and are consistent with expectations from previous studies. For example, results for $F(r)$ show approximately exponential decay [$F(r) \simeq F_0 \exp(-r/\zeta)$] in the plastic-flow regime, where the length scale ζ corresponds to the typical avalanche size and F_0 is maximal at $\gamma \simeq \gamma_{yield}$ as is typical of amorphous materials.[22,34] Results for $G(n)$ and $K(n)$ show increasing correlation on scales up to $n \sim N_e$ as systems approach fracture.[41,56] These correlations have a clear albeit gradual crossover between slow decay for $n \lesssim N_e$ and faster decay for $n \gtrsim N_e$; note that the crossover is gradual rather than sharp because entanglement spacings are broadly distributed in undeformed melts and glasses[60] and then evolve during deformation.[72,73]

Both spatial and topological measures of plasticity [i.e., $F(r)$ and $G(n)$] are clearly much more correlated in tightly entangled systems. This is not surprising; it merely indicates the much greater importance of long-range intrachain stress transmission mechanisms (e.g., covalent bond tension) in these systems. However, it is useful to contrast the γ-dependencies of these measures. Tightly entangled systems' D^2_{min} is maximally spatially correlated at $\gamma \simeq \gamma_{yield}$ but maximally topologically correlated at $\gamma \simeq \gamma_{frac}$. This distinction indirectly supports the notion that polymer glasses yield when their "primary network"[26,27,74] of short-ranged van der Waals interactions fails but that in ductile polymers the entanglement network stabilizes further relatively homogeneous deformation until ultimate failure via chain pullout and scission.[1,2]

4. DISCUSSION AND CONCLUSIONS

In this paper, we examined how chain stiffness affects shear deformation mechanisms in model polymer glasses using modern plasticity metrics. We isolated the effects of chain stiffness from competing chain thickness effects[14,16] by studying a model in which thickness is fixed and the critical parameter l_K/p monotonically increases with increasing stiffness. Our key findings were as follows: (i) flexible-chain systems are more prone to localized yielding via shear banding, while semiflexible-chain systems exhibit more spatially homogeneous yielding behavior; (ii) flexible-chain systems fail gradually and homogeneously via chain pullout, while semiflexible-chain systems fail violently at well-defined fracture planes via chain scission; (iii) the heterogeneity of systems' plastic deformation increases sharply at the onset of bond scission; (iv) although free-volume- and nonaffine-deformation-based measures of plasticity both evolve dramatically during deformation, they are not strongly correlated to each other; (v) long-range stress-transmission in tightly entangled systems makes their plasticity more spatially and topologically correlated and thus suppresses strain localization. Findings (i) and (ii) generally accord with the established-consensus view of how chain stiffness influences shear deformation by setting the tightness of the entanglement mesh;[8,12,13] here we have formulated (ii) more precisely by showing how the onset of chain scission triggers the mechanical

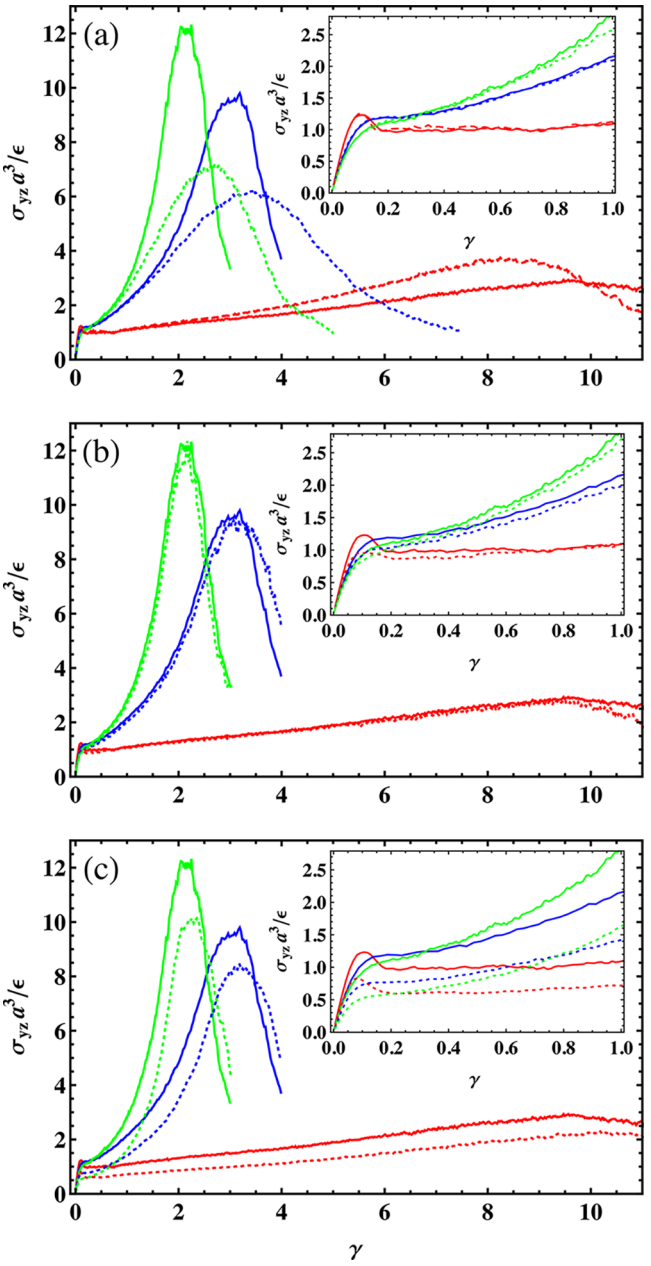

Figure 7. Effects of chain length, preparation protocol, and finite temperature on the stress−strain curves $\sigma_{yz}(\gamma)$. Red, blue, and green respectively indicate data for systems with k_{bend}/ϵ = 0, 2, and 4. Solid curves show the same results reported in Figure 1a. The dashed curves in panel a show results for flexible $N = 40N_e$ systems. Dotted curves show results for (a) shorter, $N = 8.6N_e$ chains; (b) rapidly quenched systems cooled to $T = 0$ at $|\dot{T}| = 10^{-3}/\tau$; and (c) systems deformed at $T = 3T_g/4$ (where T_g values are given in Table 1). In all panels, insets highlight the small-strain response.

instability that produces strain localization and ultimately leads to fracture. The most novel aspect of our work is that we have related these more-macroscopic trends directly to findings iii−v, which are more microscopic (i.e., have smaller characteristic length scales) and are thus more difficult to observe in experiments. Taken together, our results indicate that the additional stress transmission mechanisms provided by the greater covalent bond tensions present in tightly entangled systems act to delocalize strain and promote more homoge-

DOI: 10.1021/acs.macromol.8b00651
Macromolecules 2018, 51, 4370−4380

neous deformation than is found in loosely entangled systems, *but only until chain scission begins.*

Many of the chain-stiffness-dependent differences reported herein may be understood in terms of corresponding differences in segmental packing. Larger values of l_K/p correspond to greater interchain interpenetration on the segmental scale. Since our flexible-chain systems have larger elastic moduli owing to their more efficient segmental packing,[3,70,75] yet less interchain interpenetration, they are naturally more prone to shear banding. In contrast, our semiflexible-chain systems' less efficient packing and greater interchain interpenetration make them dilate less at small strains. Combined with their intrinsically stronger strain hardening response, this stabilizes them against shear banding. At larger strains, flexible-chain systems' lesser interchain interpenetration facilitates their ultimate failure via chain pullout, while semiflexible-chain systems' tighter entanglement (associated with their larger l_K/p[7,8,10]) favors their more violent chain-scission-dominated failure. All these results are consistent with Haward's idea[12] that the dominant parameter controlling polymer glasses' large-strain response is the density $\rho_c \sim (l_K/p)^3$ of uncrossable chain contours.

Here we focused on slowly cooled, relatively well-aged[46] glasses that occupy the lower regions of their energy landscapes prior to deformation. We focused on the low-temperature limit of these glasses' mechanical response because plasticity is simplest to interpret when it is purely strain-activated. Future work will examine how thermal and thermal-history effects couple to the chain-stiffness effects discussed herein, as well as how the micromechanisms of shear deformation through fracture couple to microscale structural features such as elastic heterogeneity[21,30,31,62−64] and/or "softness".[22,33] A brief discussion of these issues and some preliminary results are given in the Appendix.

APPENDIX. SENSITIVITY OF RESULTS TO CHAIN LENGTH, TEMPERATURE, AND PREPARATION PROTOCOL

It has long been known that chain length is a critical parameter determining polymer glasses' mechanical properties. Under typical experimental conditions, short chains ($N \lesssim 10N_e$) favor failure via chain pullout, while long chains ($N \gtrsim 10N_e$) favor failure via chain scission.[1] Above, we considered $N = 600$ systems which respectively have $N/N_e = 8.6$, 40, and 43 for $k_{bend}/\epsilon = 0$, 2, and 4. We implicitly assumed that we were considering the long-chain limit. To check the validity of this assumption, we tested the response of systems with $N/N_e = 8.6$, i.e., with $N = 600$, 128, and 120 for $k_{bend}/\epsilon = 0$, 2, and 4, and also of $k_{bend} = 0$ systems with $N/N_e = 40$ ($N = 2800$). All simulations were conducted using the same protocols described in section 2. Stress−strain curves for all these systems are compared in Figure 7a. As expected, results for all chain lengths are near-identical at small and moderate strains. Only in the dramatic hardening regime where energetic contributions to stress become significant (and especially so for tightly entangled systems[56]) does significant N-dependence of $\sigma_{yz}(\gamma)$ appear. Longer-chain systems show a greater degree of strain hardening and ultimately fracture more violently. This is expected since chain pullout is suppressed in these systems.[42] Critically, however, differences between the responses of the $N/N_e = 40$ systems are qualitatively the same as those discussed in section 3; flexible systems still exhibit a more pullout-dominated, homogeneous fracture phenomenology than their semiflexible counterparts. Note that the large N/N_e values at which the long-chain limit is reached in this study probably owe much to the Kremer−Grest model's low monomeric friction coefficient.[36,40] Conclusively determining how the phenomena discussed herein depend on chain length will require studying a wide range of model (or better yet, real) polymers and is beyond our scope.

Another factor which is well-known[13,46] to strongly affect polymer glasses' mechanical response is their preparation protocol. Systems that were prepared by rapid thermal quenches or have been mechanically rejuvenated generally display minimal strain softening and maximal ductility, while systems prepared by slow cooling from the melt followed by significant aging below T_g display opposite trends.[14,25] The preparation protocol described in section 2 produces the best-aged systems readily attainable given current computer power. Panel b contrasts their response to that of systems obtained via rapid ($|\dot{T}| = 10^{-3}/\tau$) quenches from $T = \epsilon/k_B$ to $T = 0$. Differences in the mechanical response at small strains are typical of those observed in experiments;[13,14] quenched systems strain-soften less and exhibit more diffuse shear bands than their annealed counterparts. At larger strains, differences in $\sigma_{yz}(\gamma)$ are considerably smaller, consistent with the common view that yielding rejuvenates glasses. Interestingly, however, some differences persist further beyond yield. For example, $\langle D^2_{min}(\gamma)\rangle$ values remain larger for the fast-quenched systems; their smaller $\sigma/\langle D^2_{min}\rangle$ ratios reflect the fact that less-aged glasses sit higher on their energy landscapes and are locally "softer".[30,31,46,76,77] These differences may have broad implications for the character of plastic deformation in these systems. For example, ref 78 concluded that the cooperativity of plastic deformation processes in polymer glasses scales with ρ_e based on the different strain-rate dependencies of the mechanical responses of PS−PPO blends with different ρ_e. The preparation-protocol dependence of $\sigma_{yz}(\gamma)$ illustrated here is markedly stronger for $k_{bend} = 0$ systems than for their semiflexible counterparts, suggesting that it will be of particular interest to test the ideas of ref 78 by comparing the $\dot{\gamma}$ dependencies of the mechanical responses of bead−spring systems (with different l_K/p) prepared using the same protocol.

Finally, polymer glasses' mechanical response does of course vary strongly with temperature. While a detailed consideration of thermal effects is beyond the scope of this paper, we demonstrate here that results obtained for the $T = 0$ limit are not irrelevant to typical ambient conditions. Panel c contrasts the $T = 0$ results to those for $T = 3T_g/4$, a typical value of T_{room}/T_g for many synthetic polymers.[25] At the high strain rate considered here ($\dot{\gamma} = 2.5 \times 10^{-4}/\tau$), differences are quantitative rather than qualitative. For example, greater thermal activation facilitates chain pullout and reduces bond scission, which in turn increases γ_{frac}, but the strength of these effects does not strongly couple to chain stiffness. Future work will examine thermal and rate effects in greater detail.

AUTHOR INFORMATION

Corresponding Author

*E-mail: rshoy@usf.edu (R.S.H.).

ORCID

Robert S. Hoy: 0000-0003-0283-8117

Notes

The authors declare no competing financial interest.

DOI: 10.1021/acs.macromol.8b00651
Macromolecules 2018, 51, 4370−4380

■ ACKNOWLEDGMENTS

Mark O. Robbins, Ralf Everaers, and Gary S. Grest provided helpful discussions. This material is based upon work supported by the National Science Foundation under Grant DMR-1555242.

■ REFERENCES

(1) Kramer, E. J. Microscopic and molecular fundamentals of crazing. *Adv. Polym. Sci.* **1983**, *52-53*, 1.
(2) Vincent, P. I. The tough-brittle transition in thermoplastics. *Polymer* **1960**, *1*, 425−44.
(3) Wellinghoff, S. T.; Baer, E. Microstructure and its relationship to deformation processes in amorphous polymer glasses. *J. Appl. Polym. Sci.* **1978**, *22*, 2025.
(4) Henkee, C. S.; Kramer, E. J. Crazing and shear deformation in crosslinked polystyrene. *J. Polym. Sci., Polym. Phys. Ed.* **1984**, *22*, 721−737.
(5) G'Sell, C.; Boni, S.; Shrivastava, S. Application of the plane simple shear test for determination of the plastic behavior of solid polymers at large strains. *J. Mater. Sci.* **1983**, *18*, 903.
(6) Fetters, L. J.; Lohse, D. J.; Richter, D.; Witten, T. A.; Zirkel, A. *Macromolecules* **1994**, *27*, 4639.
(7) Fetters, L. J.; Lohse, D. J.; Graessley, W. W. Chain dimensions and entanglement spacings in dense macromolecular systems. *J. Polym. Sci., Part B: Polym. Phys.* **1999**, *37*, 1023.
(8) Fetters, L. J.; Lohse, D. J.; Milner, S. T.; Graessley, W. W. Packing length influence in linear polymer melts on the entanglement, critical, and reptation molecular weights. *Macromolecules* **1999**, *32*, 6847.
(9) van Melick, H. G. H.; Govaert, L. E.; Meijer, H. E. H. On the origin of strain hardening in glassy polymers. *Polymer* **2003**, *44*, 2493.
(10) Everaers, R.; Sukumaran, S. K.; Grest, G. S.; Svaneborg, C.; Sivasubramanian, A.; Kremer, K. Rheology and microscopic topology of entangled polymeric liquids. *Science* **2004**, *303*, 823.
(11) Kramer, E. J. Open questions in the physics of deformation of polymer glasses. *J. Polym. Sci., Part B: Polym. Phys.* **2005**, *43*, 3369.
(12) Haward, R. N. Strain-hardening of thermoplastics. *Macromolecules* **1993**, *26*, 5860.
(13) Haward, R. N., Young, R. J., Eds.; *The Physics of Glassy Polymers*, 2nd ed.; Chapman and Hall: London, 1997.
(14) Meijer, H. E. H.; Govaert, L. E. Mechanical performance of polymer systems: The relation between structure and properties. *Prog. Polym. Sci.* **2005**, *30*, 915.
(15) Wu, S. Chain structure and entanglement. *J. Polym. Sci., Part B: Polym. Phys.* **1989**, *27*, 723.
(16) Wu, S. Chain structure, phase morphology, and toughness relationships in polymers and blends. *Polym. Eng. Sci.* **1990**, *30*, 753.
(17) Wang, S. On chain statistics and entanglement of linear flexible polymer melts. *Macromolecules* **2007**, *40*, 8684.
(18) Matsumiya, Y.; Watanabe, H. Nonlinear Stress Relaxation of Miscible Polyisoprene/Poly(p-tert- butylstyrene) Blends in Pseudo-monodisperse State. *Macromolecules* **2016**, *49*, 4544.
(19) Anand, L.; Gurtin, M. E. A theory of amorphous solids undergoing large deformations, with application to polymeric glasses. *Int. J. Solids Struct.* **2003**, *40*, 1465.
(20) Klompen, E. T. J.; Engels, T. A. P.; Govaert, L. E.; Meijer, H. E. H. Modeling of the postyield response of glassy polymers: Influence of thermomechanical history. *Macromolecules* **2005**, *38*, 6997.
(21) Schoenholz, S. S.; Liu, A. J.; Riggleman, R. A.; Rottler, J. Understanding plastic deformation in thermal glasses from single-soft-spot dynamics. *Phys. Rev. X* **2014**, *4*, 031014.
(22) Cubuk, E. D.; et al. Structure-property relationships from universal signatures of plasticity in disordered solids. *Science* **2017**, *358*, 1033.
(23) Lee, H. N.; Riggleman, R. A.; de Pablo, J. J.; Ediger, M. D. Deformation-Induced Mobility in Polymer Glasses during Multistep Creep Experiments and Simulations. *Macromolecules* **2009**, *42*, 4328.
(24) Bending, B.; Christison, K.; Ricci, J.; Ediger, M. D. Measurement of Segmental Mobility during Constant Strain Rate Deformation of a Poly(methyl methacrylate) Glass. *Macromolecules* **2014**, *47*, 800−806.
(25) Roth, C. B., Ed.; *Polymer Glasses*; CRC Press: 2016.
(26) Wang, S.-Q.; Cheng, S. W.; Lin, P. P.; Li, X. X. A phenomenological molecular model for yielding and brittle-ductile transition of polymer glasses. *J. Chem. Phys.* **2014**, *141*, 094905.
(27) Li, X. X.; Wang, S.-Q. Mapping brittle and ductile behaviors of polymeric glasses under large extension. *ACS Macro Lett.* **2015**, *4*, 1110.
(28) Archer, J. S.; Lesser, A. J. Shear band formation and mode II fracture of polymeric glasses. *J. Polym. Sci., Part B: Polym. Phys.* **2011**, *49*, 103.
(29) Falk, M. L.; Langer, J. S. Dynamics of viscoplastic deformation in amorphous solids. *Phys. Rev. E: Stat. Phys., Plasmas, Fluids, Relat. Interdiscip. Top.* **1998**, *57*, 7192.
(30) Manning, M. L.; Liu, A. J. Vibrational modes identify soft spots in a sheared disordered packing. *Phys. Rev. Lett.* **2011**, *107*, 108302.
(31) Smessaert, A.; Rottler, J. Correlation between rearrangements and soft modes in polymer glasses during deformation and recovery. *Phys. Rev. E* **2015**, *92*, 052308.
(32) Nicolas, A.; Rottler, J.; Barrat, J. Spatiotemportal correlations between plastic events in the shear flow of athermal amorphous solids. *Eur. Phys. J. E: Soft Matter Biol. Phys.* **2014**, *37*, 50.
(33) Cubuk, E. D.; Schoenholz, S. S.; Rieser, J. M.; Malone, B. D.; Rottler, J.; Durian, D. J.; Kaxiras, E.; Liu, A. J. Identifying structural flow defects in disordered solids using machine-learning methods. *Phys. Rev. Lett.* **2015**, *114*, 108001.
(34) Uhl, J. T.; et al. Universal quake statistics: from compressed nanocrystals to earthquakes. *Sci. Rep.* **2015**, *5*, 16493.
(35) Shavit, A.; Riggleman, R. A. Strain localization in glassy polymers under cylindrical confinement. *Phys. Chem. Chem. Phys.* **2014**, *16*, 10301.
(36) Kremer, K.; Grest, G. S. Dynamics of entangled linear polymer melts - a molecular dynamics simulation. *J. Chem. Phys.* **1990**, *92*, 5057.
(37) Rottler, J. Fracture in glassy polymers: a molecular modeling perspective. *J. Phys.: Condens. Matter* **2009**, *21*, 463101.
(38) Plimpton, S. Fast parallel algorithms for short-range molecular dynamics. *J. Comput. Phys.* **1995**, *117*, 1.
(39) Auhl, R.; Everaers, R.; Grest, G. S.; Kremer, K.; Plimpton, S. J. Equilibration of long chain polymer melts in computer simulations. *J. Chem. Phys.* **2003**, *119*, 12718.
(40) The increases in strain hardening and fracture stress and the decrease in fracture strain with increasing k_{bend} and increasing N/N_e shown in Figures 1, 2, and 7 are stronger than in previous studies[37,41,42] because we equilibrate systems at $T = T_g + 0.1\epsilon/k_B$ rather than equilibrating at $T = 1.0\epsilon/k_B$ as was the common practice prior to 2016.[43]
(41) Rottler, J.; Robbins, M. O. Growth, microstructure, and failure of crazes in glassy polymers. *Phys. Rev. E: Stat. Phys., Plasmas, Fluids, Relat. Interdiscip. Top.* **2003**, *68*, 011801.
(42) Ge, T.; Robbins, M. O.; Perahia, D.; Grest, G. S. Healing of polymer interfaces: Interfacial dynamics, entanglements, and strength. *Phys. Rev. E* **2014**, *90*, 012602.
(43) Grest, G. S. Communication: Polymer entanglement dynamics: Role of attractive interactions. *J. Chem. Phys.* **2016**, *145*, 141101.
(44) Hoy, R. S.; Foteinopoulou, K.; Kröger, M. Topological analysis of polymeric melts: Chain-length effects and fast-converging estimators for entanglement length. *Phys. Rev. E* **2009**, *80*, 031803.
(45) Sliozberg, Y. R.; Hoy, R. S.; Mrozek, R. A.; Lenhart, J. L.; Andzelm, J. W. Role of entanglements and bond scission in high strain-rate deformation of polymer gels. *Polymer* **2014**, *55*, 2543.
(46) Strum, L. C. E. Physical aging in plastics and other glassy materials. *Polym. Eng. Sci.* **1977**, *17*, 165.
(47) Warren, M.; Rottler, J. Simulations of aging and plastic deformation in polymer glasses. *Phys. Rev. E* **2007**, *76*, 031802.
(48) Rottler, J.; Warren, M. Deformation, yield and ageing in glassy solids. *Eur. Phys. J.: Spec. Top.* **2008**, *161*, 55.

DOI: 10.1021/acs.macromol.8b00651
Macromolecules 2018, 51, 4370−4380

(49) Rottler, J.; Robbins, M. O. Shear yielding of amorphous polymer glasses: effect of temperature and strain rate. *Phys. Rev. E: Stat. Phys., Plasmas, Fluids, Relat. Interdiscip. Top.* **2003**, *68*, 011507.
(50) Gilman, J. J. Mechanical behavior of metallic glasses. *J. Appl. Phys.* **1975**, *46*, 1625.
(51) Ge, T.; Pierce, F.; Perahia, D.; Grest, G. S.; Robbins, M. O. Molecular dynamics simulations of polymer welding: strength from interfacial entanglements. *Phys. Rev. Lett.* **2013**, *110*, 098301.
(52) Uchida, N.; Grest, G. S.; Everaers, R. Viscoelasticity and primitive path analysis of entangled polymer liquids: From F-actin to polyethylene. *J. Chem. Phys.* **2008**, *128*, 044902.
(53) Nguyen, H. T.; Smith, T. B.; Hoy, R. S.; Karayiannis, N. C. Effect of chain stiffness on the competition between crystallization and glass- formation in model unentangled polymers. *J. Chem. Phys.* **2015**, *143*, 144901.
(54) Hasan, O. A.; Boyce, M. C. A constitutive model for the nonlinear viscoelastic viscoplastic behavior of glassy polymers. *Polym. Eng. Sci.* **1995**, *35*, 331.
(55) Hoy, R. S.; Robbins, M. O. Strain hardening of polymer glasses: Entanglements, energetics, and plasticity. *Phys. Rev. E* **2008**, *77*, 031801.
(56) Hoy, R. S. Why is understanding glassy polymer mechanics so difficult? *J. Polym. Sci., Part B: Polym. Phys.* **2011**, *49*, 979.
(57) Arruda, E. M.; Boyce, M. C. Evolution of plastic anisotropy in amorphous polymers during finite straining. *Int. J. Plast.* **1993**, *9*, 697.
(58) Boyce, M. C.; Arruda, E. M.; Jayachandran, R. The large-strain compression, tension, and simple shear of polycarbonate. *Polym. Eng. Sci.* **1994**, *34*, 716.
(59) Svaneborg, C.; Grest, G. S.; Everaers, R. Disorder effects on the strain response of model polymer networks. *Polymer* **2005**, *46*, 4283.
(60) Tzoumanekas, C.; Theodorou, D. N. Topological analysis of linear polymer melts: A statistical approach. *Macromolecules* **2006**, *39*, 4592.
(61) Humphrey, W.; Dalke, A.; Schulten, K. VMD: Visual molecular dynamics. *J. Mol. Graphics* **1996**, *14*, 33.
(62) Smessaert, A.; Rottler, J. Structural relaxation in glassy polymers predicted by soft modes: a quantitative analysis. *Soft Matter* **2014**, *10*, 8533.
(63) Riggleman, R. A.; Douglas, J. F.; de Pablo, J. J. Antiplasticization and the elastic properties of glass-forming polymer liquids. *Soft Matter* **2010**, *6*, 292.
(64) Makke, A.; Perez, M.; Rottler, J.; Lame, O.; Barrat, J. L. Predictors of Cavitation in Glassy Polymers under Tensile Strain: A Coarse-Grained Molecular Dynamics Investigation. *Macromol. Theory Simul.* **2011**, *20*, 826.
(65) Wang, S.-Q.; Ravindranath, S.; Wang, Y.; Boukany, P. New theoretical considerations in polymer rheology: elastic breakdown of chain entanglement network. *J. Chem. Phys.* **2007**, *127*, 064903.
(66) Yaoita, T.; Isaki, T.; Masubuchi, Y.; Watanabe, H.; Ianniruberto, G.; Marrucci, G. Primitive chain network simulation of elongational flows of entangled linear chains: Stretch/orientation-induced reduction of monomeric friction. *Macromolecules* **2012**, *45*, 2773.
(67) Schweizer, K. S.; Sussman, D. M. A force-level theory of the rheology of entangled rod and chain polymer liquids. I. Tube deformation, microscopic yielding, and the nonlinear elastic limit. *J. Chem. Phys.* **2016**, *145*, 214903.
(68) Salerno, K. M.; Maloney, C. E.; Robbins, M. O. Avalanches in Strained Amorphous Solids: Does Inertia Destroy Critical Behavior? *Phys. Rev. Lett.* **2012**, *109*, 105703.
(69) Kumar, V. S.; Kumaran, V. Voronoi cell volume distribution and configurational entropy of hard-spheres. *J. Chem. Phys.* **2005**, *123*, 114501.
(70) Kumar, R.; Goswami, M.; Sumpter, B. G.; Novikov, V. N.; Sokolov, A. P. Effects of backbone rigidity on the local structure and dynamics in polymer melts and glasses. *Phys. Chem. Chem. Phys.* **2013**, *15*, 4604.
(71) Derlet, P. M.; Maass, R. Linking high- and low-temperature plasticity in bulk metallic glasses II: use of a log-normal barrier energy distribution and a mean-field description of high-temperature plasticity. *Philos. Mag.* **2014**, *94*, 2776.
(72) Leonforte, F. Evolution of entanglements during the response to a uniaxial deformation of lamellar triblock copolymers and polymer glasses. *Phys. Rev. E* **2010**, *82*, 041802.
(73) Ge, T.; Tzoumanekas, C.; Anogiannakis, S. D.; Hoy, R. S.; Robbins, M. O. Entanglements in Glassy Polymer Crazing: Cross-Links or Tubes? *Macromolecules* **2017**, *50*, 459.
(74) Li, X.; Liu, J.; Liu, Z.; Tsige, M.; Wang, S. Illustrating the Molecular Origin of Mechanical Stress in Ductile Deformation of Polymer Glasses. *Phys. Rev. Lett.* **2018**, *120*, 077801.
(75) Ness, C.; Palyulin, V. V.; Milkus, R.; Elder, R.; Sirk, T.; Zaccone, A. Nonmonotonic dependence of polymer-glass mechanical response on chain bending stiffness. *Phys. Rev. E: Stat. Phys., Plasmas, Fluids, Relat. Interdiscip. Top.* **2017**, *96*, 030501.
(76) Stillinger, F. H. A Topographic View of Supercooled Liquids and Glass-Formation. *Science* **1995**, *267*, 1935.
(77) Rodney, D.; Schroder, T. On the potential energy landscape of supercooled liquids and glasses. *Eur. Phys. J. E: Soft Matter Biol. Phys.* **2011**, *34*, 100.
(78) Ho, J.; Govaert, L. E.; Utz, M. Plastic deformation of glassy polymers: correlation of shear activation volume and entanglement density. *Macromolecules* **2003**, *36*, 7398.

DOI: 10.1021/acs.macromol.8b00651
Macromolecules 2018, 51, 4370−4380